

A Global Mean Dynamic Ocean Topography

Frank Siegismund¹

¹Technical University Munich

November 23, 2022

Abstract

The space-born geodetic temporal Mean Dynamic Topography (MDT) is obtained from the difference of altimetric Mean Sea Surface (MSS) η and the geoid height N . With the geostrophic surface currents obtained from its gradient the MDT is an essential parameter when describing the ocean dynamics. Spectral consistency of η and N is crucial to minimize MDT errors. Usually, η is globalized to allow for a Spherical Harmonic (SH) analysis and small scales beyond maximum degree and order (d/o) resolved in the geoid are cut-off. However, the usual globalization causes ocean-land steps in $\eta-N$ and spectral inconsistencies of N and η over land. To overcome both issues a new methodology is proposed based on globalization of the MDT. A Laplacian smoother with the coastal MDT values as boundary condition is applied resulting in a flat surface over land and a continuous ocean-land transition. The new methodology strongly reduces Gibbs effects and the need to work with high resolution MDTs to minimize them. Reduction of resolution is tested to reduce MDT uncertainties caused by the commission error expected to increase with decreasing scale. Applying drifter data and a high resolution hydrodynamic ocean model it is shown, that for the Gulf Stream and the Kuroshio geodetic MDTs applying recent combined geoid models contain physical information up to at least d/o 420 (48km spatial scale). Since for oceanic regions with strong gradients in N still inconsistencies between the geoid and the MSS exist, it depends on application/region if a higher resolution MDT is needed.

A Global Mean Dynamic Ocean Topography

F. Siegismund¹

¹Inst. Astr. & Phys.Geodesy, Technische Universität München, Munich, Germany

Key Points:

- The proposed new methodology for land-filling the Mean Sea Surface (MSS) strongly reduces Gibbs effects in the Mean Dynamic Topography (MDT).
- Recent geoid models contain physical information at least up to maximum degree and order (d/o) 420 corresponding to 48km length scale.

Corresponding author: Frank Siegismund, frank.siegismund@tum.de

Abstract

The space-born geodetic temporal Mean Dynamic Topography (MDT) is obtained from the difference of altimetric Mean Sea Surface (MSS) h and the geoid height N . With the geostrophic surface currents obtained from its gradient the MDT is an essential parameter when describing the ocean dynamics. Spectral consistency of h and N is crucial to minimize MDT errors. Usually, h is globalized to allow for a Spherical Harmonic (SH) analysis and small scales beyond maximum degree and order (d/o) resolved in the geoid are cut-off. However, the usual globalization causes ocean-land steps in $h-N$ and spectral inconsistencies of N and h over land. To overcome both issues a new methodology is proposed based on globalization of the MDT. A Laplacian smoother with the coastal MDT values as boundary condition is applied resulting in a flat surface over land and a continuous ocean-land transition. The new methodology strongly reduces Gibbs effects and the need to work with high resolution MDTs to minimize them. Reduction of resolution is tested to reduce MDT uncertainties caused by the commission error expected to increase with decreasing scale. Applying drifter data and a high resolution hydrodynamic ocean model it is shown, that for the Gulf Stream and the Kuroshio geodetic MDTs applying recent combined geoid models contain physical information up to at least d/o 420 (48km spatial scale). Since for oceanic regions with strong gradients in N still inconsistencies between the geoid and the MSS exist, it depends on application/region if a higher resolution MDT is needed.

1 Introduction

The ocean Dynamic Topography (DT) is a powerful parameter in oceanography. It is defined as the deviation of the geometrical ocean surface from the geoid, which itself is that equipotential surface of gravity closest to the ocean surface in a least-squares sense. Defined like this the geostrophic surface currents follow the isolines of the DT and their strength is determined from the gradient of the DT and the local Coriolis parameter. The geostrophic currents are the equilibrium of horizontal pressure and Coriolis force and quite accurately describe the circulation on large spatial (>1000 km) and temporal (few days and longer) scales.

Applying space-born observations, global maps of the temporal Mean DT (MDT) can be determined as the difference of the temporal mean geometric surface of the ocean h observed from altimetry and the geoid N obtained from gravity measurements. This observation strategy is very powerful providing global maps of a very useful parameter for oceanography that hardly can be obtained by other means. In recent years the U.S./German GRACE (Tapley et al., 2004), recently extended by its Follow-On, and the ESA GOCE (Rummel et al., 2002) satellite missions have provided high precision gravimetric measurements with respective improvements in the accuracy of gravity-based geoids. Satellite-only geoid models are now available up to degree and order (d/o) 300, corresponding to 67 km spatial resolution. Combined geoid models in addition utilize altimetry data and terrestrial gravity data up to a $5' \times 5'$ grid, which corresponds/results in gravity field models and geoids up to approximately d/o 2160.

The computation of the MDT as the difference of h and N , however, is a challenging task since this difference is two orders of magnitude smaller than the two almost identical parameters. In addition, observation strategies and physical nature of the two quantities differ. h is observed as a geometrical quantity and naturally provided on an ocean-only grid, whereas the geoid is a global linear functional of the Earth's gravity potential provided usually in spectral space as Stokes coefficients which result from projecting the potential onto Spherical Harmonic (SH) functions. The small deviation between h and N and comparable or higher spectral power in N compared to the MDT also for small spatial scales makes spectral consistency of N and h a central issue for the quality of the resulting MDT.

60 The usual strategy for a spectrally consistent combination of h and N to obtain
 61 the MDT is the spectral approach as described by Bingham et al. (2008). Here h has to
 62 be globalized which needs a filling-in of land values. Then spectral consistency is estab-
 63 lished by SH analysis, cutting-off the Stokes coefficients for SH functions above maxi-
 64 mum d/o n of the applied geoid model and synthesizing back to a desired grid in phys-
 65 ical space. Subtraction of N from the globalized and filtered h_n provides the MDT, that
 66 is finally spatially filtered if needed.

67 For the necessary filling-in of land data, usually geoid height from a specific geopo-
 68 tential model is applied. Either the MSS is already provided as global field by the pro-
 69 ducer and is used unchanged (Sanchez-Reales et al., 2013; Knudsen et al., 2011) or that
 70 geoid model is applied which is later also subtracted from the MSS to obtain the MDT
 71 (Feng et al., 2013; Sanchez-Reales et al., 2016). Though this filling-in with geoid data
 72 is very convenient, it causes two sources of errors when subsequently applying the spec-
 73 tral filter to the globalized MSS:

- 74 1. An ocean-land step is inevitable since the MSS is the sum of geoid and MDT while
 75 over land only geoid height is set,
- 76 2. the geoid data used for land-fill-in is usually spectrally inconsistent with the geoid
 77 contained in the MSS over the ocean.

78 Both issues will cause unphysical wavy noise to spread into the ocean when a spectral
 79 cut-off filter is applied. This noise is increasing with decreasing cut-off d/o. The chal-
 80 lenges caused by the step in MDT along the coastlines are analysed in Albertella and
 81 Rummel (2009). Both issues, the ocean-land step as well as the spectral inconsistency
 82 of land and ocean geoid, are tackled in this paper applying an easy to implement approach.
 83 The fundamental idea is to understand the MDT as a global field and to define land val-
 84 ues as function of the ocean values with the objective to minimize unphysical signals over
 85 the ocean when (spectral) filtering is applied. Though it isn't claimed that the objec-
 86 tive is fulfilled completely it is shown that the proposed approach solves the dominant
 87 ocean-land step problem and by this strongly reduces wavy structures which are com-
 88 mon artefacts in low resolution MDT solutions generally caused by small scale informa-
 89 tion in $h - N$ that is not resolved in the low resolution MDT.

90 Beside the globalization of h , still following the spectral approach (Bingham et al.,
 91 2008), the cut-off maximum d/o of the MDT has to be selected. So far this selection is
 92 dominated by the mentioned wavy structure of Gibbs effects caused by the inability to
 93 reproduce the ocean-land step with limited spatial resolution, which increases with de-
 94 creasing maximum d/o and is the dominant error component in low resolution MDTs.
 95 Thus high resolution is needed though both the commission error in geoid and MSS is
 96 expected to increase with decreasing spatial scale and it isn't known up to which reso-
 97 lution the geodetic MDT actually contains physical information.

98 With the proposed globalization strategy for h and thereby substantial reduction
 99 of noise in low resolution MDT solutions, the trade-off of increasing commission and de-
 100 creasing omission error with increasing spectral resolution comes into focus when select-
 101 ing the maximum d/o of the dedicated MDT. To provide useful information about sig-
 102 nal content in the small scales of recent geoid models is thus the second subject of this
 103 paper. This issue is interesting by itself and will facilitate the appropriate choice of the
 104 cut-off d/o in practical applications.

105 The remaining paper is organized as follows: In section 2 the general methodol-
 106 ogy to compute an MDT and the applied models for h and N are introduced. For the
 107 assessment of surface geostrophic currents obtained from the MDTs we compare with
 108 both near-surface drifter data and results from a high-resolution hydrodynamic ocean
 109 model of the North Atlantic. Both tools are explained in this section. In section 3 the
 110 methodology for globalizing the MSS is introduced. The MDTs and geostrophic surface

111 currents derived by this approach are assessed by comparison to other commonly used
 112 methods. Section 4 is dedicated to small scale signal content in MDTs derived apply-
 113 ing recent high-resolution combined geoid models. It is tested to what extent the geostrophic
 114 surface currents of the strongest Western boundary currents, the Gulf Stream and the
 115 Kuroshio, are reproduced depending on resolution of the MDTs. These currents are se-
 116 lected since here the resolution down to small scales is needed to resolve the full current
 117 due to the short across-scale of the currents. In addition, the uncertainty in currents caused
 118 by the commission error in both the MSS and the geoid has as low as possible weight
 119 due to the large signal strength. In section 5 a conclusion of the main outcomes is pro-
 120 vided.

121 2 Methodology and Approach

122 2.1 Mean Dynamic Topography

123 The geodetic MDTs in this paper are computed as deviation of the MSS from the
 124 geoid model. Both, MSS and geoid model use the same tide system (tide-free) and ref-
 125 erence ellipsoid (TOPEX). The methodology then follows the spectral approach as de-
 126 scribed in Bingham et al. (2008). In this approach the globalized MSS model is projected
 127 to SH functions, cut-off at a specific maximum d/o selected for the MDT and synthe-
 128 sized to a grid the MDT is desired on. Then the geoid is synthesized to the same max-
 129 imum d/o and grid, and subtracted from the MSS. The resulting MDT is spatially fil-
 130 tered if necessary. For the MSS we apply DTU15 (Andersen et al., 2016). The correc-
 131 tion of the land values in this already globalized model is a central subject of this pa-
 132 per and explained and assessed in section 3. The geoid models we apply to compute the
 133 different MDTs are listed in Table 1. They are obtained from recent gravity field mod-
 134 els available for download at the International Centre for Global Earth Models (ICGEM).
 135 For the combined models the newest releases from the different processing centers are
 136 chosen. In addition, TIM_R6 (Brockmann et al., 2014) is selected as a recent satellite-
 137 only model. The MDTs are computed on a $10' \times 10'$ grid. Spatially filtered MDTs are
 138 obtained, were needed, by applying a truncated Gaussian kernel with the truncation set
 139 at three times the filter length.

140 The low-resolution geoid model (TIM_R6) is used to compute the MDTs in sec-
 141 tion 3 applying and comparing different methods for land-filling the MSS. The effects
 142 of the proposed new methodology for this task are largest for low resolution MDTs. There-
 143 fore and since satellite-only models, specifically including GOCE mission data, have been
 144 used frequently in recent years, the TIM_R6 model is used here rather than a high res-
 145 olution combination model. The GECO model is used to calculate coastal MDT values
 146 needed for MSS land-filling with the new methodology explained in Section 3, though
 147 the other three very-high-resolution models (SGG-UGM-1, EIGEN6C4, EGM2008) were
 148 also tested and show similar results. All combination models are used in section 4 for
 149 the investigation of MDT small scale signal content.

150 With local Cartesian coordinates x and y towards east and north, respectively, the
 151 zonal (meridional) geostrophic surface currents u (v) are calculated from the MDTs as

$$152 \quad u = -\frac{g}{f} \frac{\partial \zeta}{\partial y} \quad (1)$$

$$153 \quad v = \frac{g}{f} \frac{\partial \zeta}{\partial x} \quad (2)$$

154 with g the acceleration due to gravity, ζ the MDT and $f = 2\Omega \sin\phi$ the Coriolis param-
 155 eter, where Ω is the angular speed of the earth and ϕ is the latitude. Practically, the ve-
 156 locities are computed from central MDT differences with u (v) defined on the longitudes
 157 (latitudes) of the MDT grid, but on latitudes (longitudes) centered between the two MDT
 grid points the velocity is computed from. This two-point central difference computa-
 tion of velocities minimizes smoothing. For practical reasons, the absolute velocity $w =$

Table 1. Gravity field models applied to obtain the geoid height. In the data column, the datasets used in the development of the models are summarized, where S is for satellite (e.g., GRACE, GOCE, Lageos), A is for altimetry, and G for ground data (e.g., terrestrial, shipborne and airborne measurements). If available gravity field models are applied this is also indicated (e.g., GOCC05s, EGM2008).

Model	data	degree	Reference
TIM_R6	S(GOCE)	300	Brockmann et al. (2014)
XGM2016	A,G,S(GOCC05s)	719	Pail et al. (2018)
GOCO05c	A,G,S	720	Fecher et al. (2017)
SGG-UGM-1	EGM2008, S(Goce)	2159	Liang et al. (2018)
GECCO	EGM2008, S(Goce)	2190	Gilardini et al. (2016)
EIGEN6C4	A,G,S(Goce),S(Grace),S(Lageos)	2190	Frst et al. (2014)
EGM2008	A,G,S(GRACE)	2190	Pavlis et al. (2012)

158 $\sqrt{u^2 + v^2}$ is defined on the MDT grid applying u and v north and east of the grid point,
 159 respectively.

160 2.2 Geostrophic currents from near-surface drifter data

161 The drifter data applied in this study is the 6-hourly data set as provided by the
 162 Global Drifter Program (GDP, Lumpkin and Pazos (2007)). Only drogoue-on drifters are
 163 applied (Lumpkin & Johnson, 2013). Available data until December 2014, made up of
 164 more than 10 million entries, are used. To estimate the time average surface geostrophic
 165 circulation, as can be drawn from the MDT maps, a number of corrections are neces-
 166 sary applying external data wind (NCEP/NCAR reanalysis, Kalnay et al. (1996)) and
 167 updated merged Sea Level Anomaly (SLA) provided by the Copernicus Marine Envi-
 168 ronment Monitoring Service (CMEMS). The methodology generally follows the descrip-
 169 tion in Siegismund (2013), specifically subtracting wind slip of surface buoys, the filter-
 170 ing for inertial currents and subtracting the time variable part of the geostrophic cur-
 171 rents calculated from SLA, re-referenced to the period 2002–2013 and linearly interpo-
 172 lated to the drifter positions and time.

173 However, to secure complete independence of drifter data from any MDT used in
 174 this study, the estimation of Ekman currents does not use an MDT as reference. Instead,
 175 anomalies of the filtered drifter velocities within $5^\circ \times 5^\circ$ boxes are calculated. The work
 176 of Rio and Hernandez (2003) and Ralph and Niiler (1999) is followed, but instead of the
 177 total Ekman current \vec{U}_e , the anomaly \vec{U}'_e is estimated as

$$\vec{U}'_e = b \left(\frac{\vec{\tau}}{\sqrt{f|\tau|}} \right)' e^{i\Theta} \quad (3)$$

178 with $\tau = c_d * \rho * U_w * |U_w|$ the wind stress, where $c_d = 2.7 * 10^{-3} * |U_w|^{-1} + 1.42 * 10^{-4} +$
 179 $7.64 * 10^{-5} * |U_w|$ and $|U_w|$ the wind speed. ' stands for the deviation from the mean
 180 for the considered box. b and Θ are determined by Least-squares (LS) fitting \vec{U}'_e to the
 181 drifter velocity anomalies for each box. No LS fitting is performed for boxes containing
 182 not more than 1.000 data points.

183 All other boxes are checked for unrealistic estimates of b and Θ . Therefor $1ms^{-1}$
 184 westerly wind is supposed and the Ekman current for the box and mean as well as stan-
 185 dard deviation of both vector components of the Ekman current for the surrounding 8
 186 boxes are computed. If for at least one vector component the Ekman current of the con-
 187 sidered box deviates from the mean of the surrounding boxes by more than 2.5 times the
 188 standard deviation, the LS fit is identified as outlier. The check for outliers is iterated
 189 for all boxes several times until no outlier is found anymore.

190 For those boxes with too few drifter data points for the LS fitting or where the re-
 191 sults of the fitting are detected as outliers, b and Θ are a function of the parameters in
 192 the surrounding boxes, respectively. b is obtained as weighted average. The weighting
 193 is set proportional to the reciprocal center-center distance between the boxes. To obtain
 194 Θ the Ekman currents for westerly wind are summed but with the lengths of the vec-
 195 tors corrected to the same weighting as used to calculate b . Θ is then set as $\Theta = atan(v_e/u_e)$
 196 with u_e (v_e) the zonal (meridional) component of the vector. For every data point the
 197 Ekman currents are calculated and subtracted from the filtered drifter velocities to ob-
 198 tain estimates of temporal mean geostrophic currents at the positions of the filtered drifter
 199 velocities.

200 For the calculation of surface geostrophic velocities across sections as is discussed
 201 in Section 4, all velocities from drifters crossing the section are taken into account. The
 202 velocity on the section is estimated as the average of the velocity vector before and af-
 203 ter the crossing projected to the direction perpendicular to the section. To achieve a sub-
 204 stantial averaging-out of errors, from all crossing points all possible 19 neighboring points
 205 are grouped. A weighted average of both velocity and position, is computed for each group

206 applying a reciprocal total velocity weighting (Maximenko, 2004) with the total veloc-
 207 ity the sum of geostrophic, Ekman and wind slip component.

208 RMS differences of drifter and MDT derived geostrophic velocities as discussed in
 209 Section 3 are based on evaluations for all drifter velocities in a specified region. The eval-
 210 uation includes the comparison of the zonal and the meridional velocity component. For
 211 the geostrophic velocities derived from the MDT the two components are defined on dif-
 212 ferent grids. The zonal (meridional) component is defined central between two neigh-
 213 bouring MDT grid points on the same longitude (latitude). For a specific drifter data
 214 point and component a plane is defined by the three nearest MDT grid points surround-
 215 ing the drifter data point and the value of that plane for the drifter data point is applied
 216 as MDT derived geostrophic velocity component. The (MDT-drifter) difference in sur-
 217 face geostrophic velocity is determined as

$$\Delta w = \sqrt{(\Delta u)^2 + (\Delta v)^2} \quad (4)$$

218 with Δu (Δv) the difference in the zonal (meridional) velocity component. To obtain
 219 spatial mean RMS values not biased by the uneven distribution of the drifter data points,
 220 the squared velocity differences are averaged over the boxes of a $1^\circ \times 1^\circ$ grid and then
 221 averaged over the region considered before the square root is applied.

222 2.3 Hydrodynamic Model

223 The hydrodynamic model applied is the MIT general circulation model (Marshall
 224 et al., 1997) covering the Arctic Ocean and the Atlantic Ocean north of 33°S in a hor-
 225 izontal resolution of 4 km. The model was set up with a bipolar curvilinear grid, with
 226 one pole located over North America and the other over Europe. In the vertical, the model
 227 setup uses 100 levels of varying depth, from 5 m in the upper ocean to 185 m in the deep
 228 ocean. Bottom topography is derived from the ETOPO database in $2'$ resolution. The
 229 model starts from the year 2002 conditions from another model, that has a similar set-
 230 up with lower resolution of approximately 8 km and itself starts in 1948 from the annual
 231 mean temperature and salinity from the World Ocean Atlas 2005 (Boyer et al., 2005).
 232 The model simulation spans the period from 2003 to 2009.

233 The model simulation is forced at the surface by fluxes of momentum, heat, and
 234 freshwater computed using bulk formulae and the 6 hourly atmospheric state from the
 235 1989–2009 ECMWF ERA-Interim reanalysis (Dee et al., 2011). At the open southern
 236 boundary, the simulations are forced by the output of a 1° resolution global solution of
 237 the MITgcm forced by the NCEP data set. A barotropic net inflow of 0.9 Sv ($1 \text{ Sv} = 10^6 \text{ m}^3 \text{ s}^{-1}$)
 238 into the Arctic is prescribed at Bering Strait, the models' northern open boundary, which
 239 balances a corresponding outflow through the southern boundary at 33°S . A dynamic
 240 thermodynamic sea ice model solves for sea ice parameters. See Biri et al. (2016) for de-
 241 tails.

242 For the purpose of this study the modeled sea level is saved on a $10' \times 10'$ grid ap-
 243 plying bilinear interpolation. For regions outside the model grid a Laplacian smoother
 244 is applied to obtain a global MDT. The Laplacian smoother solves the Laplacian Equa-
 245 tion $\Delta \zeta = 0$ with the MDT values at the margin of the model grid as boundary con-
 246 dition. Different spatial resolutions are realized by successive SH analysis and synthe-
 247 sis steps. Geostrophic currents are obtained with the same method as applied for the geode-
 248 tic MDTs.

249 3 Global Mean Dynamic Topography

250 Geodetic MDTs are derived from the difference of MSS and geoid height. The spec-
 251 tral inconsistency between the MSS and the geoid is usually solved by filling the land
 252 areas of the MSS with geoid information and low-pass filtering the globalized MSS by

253 performing a SH analysis and cutting off short scales above maximum d/o of the geoid.
 254 However, two sources of inconsistency remain after globalizing the MSS that cause un-
 255 physical MDT signal when cutting off small scale information in the MSS:

- 256 1. a step along the coastline with its height depending on the local amplitude of the
 257 MDT,
- 258 2. the geoid defined over land misses small scale signal contained in the MSS over
 259 the ocean

260 It is suggested here to globalize the MDT and use high resolution geoid information over
 261 land to provide an as best as possible globalization of the MSS which then massively re-
 262 duces the inconsistency.

263 3.1 Methodology

264 Over the ocean the true (error-free) MDT is defined as usual as the difference of
 265 true MSS and geoid models, respectively:

$$\zeta(x_o) = h(x_o) - N(x_o) \quad (5)$$

266 for an arbitrary ocean point x_o . To allow for a globalization that minimizes unphysical
 267 signal when cutting-off small scales, a flat continuation from ocean to land is needed. For
 268 this, we solve the Laplacian Equation

$$\Delta\zeta(x_l) = 0 \quad (6)$$

269 for all land points x_l with the coastal MDT values ζ_c as boundary condition. As result,
 270 for an arbitrary land point x_l we obtain

$$\zeta(x_l) = g(\zeta_c, x_l) \quad (7)$$

271 with g the function determined by the Laplace equation.

272 Though this MDT land definition does not ensure differentiability along the coast-
 273 lines it at least prevents Gibbs effects caused by the ocean-land step and minimizes small
 274 scale land signals that potentially could cause unphysical ocean signals when applying
 275 a spectral low-pass filter. Given the true ocean MDT, the unambitious method to fill-
 276 in land signals as described above will provide what is here called the 'true' global MDT
 277 though better filling approaches might develop with future research. The true global MDT
 278 can be projected onto SH functions and expressed as truncated MDT with arbitrary max-
 279 imum d/o $n > 0$. The necessary successive SH analysis and synthesis steps are explained
 280 in detail e.g. in Bingham et al. (2008).

281 From the globalization of the MDT, by combining Eqs. 5 and 7, a clear definition
 282 for the MSS over land follows:

$$h(x_l) = N(x_l) + \zeta(x_l) = N(x_l) + g(\zeta_c, x_l) \quad (8)$$

283 for an arbitrary land point x_l . The true global MDT truncated at maximum d/o n can
 284 then be described as

$$\zeta_n = f_n(h - N) = f_n(h) - f_n(N) \quad (9)$$

285 where f_n describes the spectral truncation of a globally defined function to maximum
 286 d/o n . The error of an MDT, defined up to some maximum d/o n in a real-life appli-
 287 cation, can be described in terms of the deviation from the 'true' MDT truncated at the
 288 same resolution as

$$\begin{aligned} e_{\zeta_n} &= \tilde{\zeta}_n - \zeta = \tilde{\zeta}_n - \zeta_n + (\zeta_n - \zeta) = (f_n(\tilde{h}) - f_n(\tilde{N})) - (f_n(h) - f_n(N)) + e_n \\ &= f_n(\tilde{h} - h) - f_n(\tilde{N} - N) + e_n = f_n(e_h) - f_n(e_N) + e_n \end{aligned} \quad (10)$$

289 with $\tilde{\cdot}$ indicating real-life application fields, e_h the error in the globalized MSS before trun-
 290 cation to the selected maximum d/o and e_N the commission error of the geoid model.
 291 $e_n = \zeta_n - \zeta$ is the omission error of the MDT caused by missing the signal beyond d/o
 292 n . f_n describes the effect of spectrally filtering the errors which causes ringing and other
 293 effects depending on spectral distribution of the error and the cut-off d/o.

294 Since the geoid is usually described as a linear functional of SH coefficients, the spec-
 295 trally filtered error of the geoid $f_n(e_N)$ is a linear function of the SH coefficients up to
 296 d/o n and independent of the $h-N$ combination strategy and not discussed here. The
 297 omission error e_n is discussed in Section 4.

298 The MSS error is described as

$$e_h = e_{h_o} + e_{N_l} + e_c \quad (11)$$

299 and after spectral filtering

$$f_n(e_h) = f_n(e_{h_o}) + f_n(e_{N_l}) + f_n(e_c) \quad (12)$$

300 e_{h_o} describes the error of the MSS over the ocean and is not discussed here (though
 301 MSS at individual points near the coast may be detected as outliers, defined as land points
 302 and then are subject to the Laplacian operator, see below). e_{N_l} and e_c are the errors of
 303 the geoid model and ζ_c , respectively, applied in Eq. 8 for land filling the MSS.

304 The suggested strategy to globalize the MSS aims in minimizing both e_{N_l} and e_c .
 305 In past applications e_c is usually equal to ζ_c since just a geoid model is already filled-
 306 in as MSS land values by the provider or later applied by the user, ignoring the MDT
 307 along the coast. The ocean-land step, which is then equal to the coastal MDT values, causes
 308 Gibbs effects described in $f_n(e_c)$ when spectrally filtering the MSS. e_{N_l} depends on the
 309 geoid model applied. Often, the same geoid model is applied that is later subtracted from
 310 $f_n(\tilde{h})$ to compute $\tilde{\zeta}_n$. If this geoid model comes as a satellite-only model it has low max-
 311 imum d/o and e_{N_l} contains the missing geoid signal between maximum d/o of the geoid
 312 model and maximum d/o of the MSS to be globalized. Spectral filtering of the MSS be-
 313 fore combination with the geoid to obtain the MDT will cause a spreading of this error
 314 to the ocean and is then seen as error in the MDT.

315 In our approach we follow Eq. 8 to globalize the MSS. To compute ζ_c we subtract
 316 a geoid model from the coastal MSS. The same geoid model is added to the globalized
 317 MDT to obtain MSS land values. In general this consistency is not necessary. Also a hy-
 318 drodynamic model could be applied to derive ζ_c . But any inconsistency of data used left
 319 and right of the coastline can cause a step in $\tilde{h} - \tilde{N}$ and is avoided here. The global-
 320 ized MSS can in general be provided in any resolution m at or above maximum d/o n
 321 of the desired MDT and is then spectrally cut as described in Eq. 8. The decision for
 322 m will depend on two issues:

- 323 1. Since any low-pass filtering is prone to Gibbs-like effects the globalization should
 324 be performed as close as possible to the resolution the MSS is originally provided
 325 with,
- 326 2. geoid information over land has to be available consistent with the chosen reso-
 327 lution m .

328 Geoid models are nowadays available up to d/o 2160 and it is recommended to use this
 329 resolution for the land-filling of the MSS. However, due to limits in available resources
 330 maximum d/o will be 1080 here, which is, however, sufficient to show the impact of the
 331 approach to the resulting MDT. It is worth noting at this point that the coastal MDT
 332 determined to globalize the MSS is not seen as physical signal in the resulting MDT in
 333 the end. It is just a mean to compute the 'land MDT' added to the geoid. It is thus not

334 inconsistent to apply the suggested MSS globalization applying a high resolution com-
 335 bined geoid model and use a satellite-only geoid model to compute the MDT at the end.

336 The suggested full procedure to compute a global MDT is as follows:

- 337 1. A gridded MSS is provided in the spectral resolution of the geoid model applied
 338 to compute the MSS land values. We apply DTU15, which is provided on a $1' \times 1'$
 339 global grid and apply a spectral analysis/synthesis step to reduce the resolution
 340 to maximum d/o 1080 computed on a $10' \times 10'$ grid.
- 341 2. The geoid chosen for the globalization/correction of the MSS is subtracted to ob-
 342 tain a high resolution MDT ζ_{hf} . We use here different geoid models, see below.
- 343 3. The land-sea mask necessary to identify the grid points that need a filling, is pro-
 344 vided by the GOCE User Toolbox (GUT), which is also applied for all analysis/synthesis
 345 and spatial filtering issues. For outlier detection the geostrophic surface currents
 346 based on the ocean points of ζ_{hf} are computed. For both current vector compo-
 347 nents, if velocity exceeds 3 ms^{-1} , the involved grid points are set to land. This
 348 is done to minimize influence of potentially large local MSS errors onto the MDT
 349 at some locations near the coast.
- 350 4. Based on the coastal values of ζ_{hf} the MDT land values $\zeta(x_l)$ are computed ap-
 351 plying the Laplacian equation.
- 352 5. $\zeta(x_l)$ is added to the geoid and used as land values for the MSS.
- 353 6. The MSS is successively analyzed/synthesized to the spectral resolution n of the
 354 resulting MDT.
- 355 7. The geoid is computed for maximum d/o n .
- 356 8. $\tilde{\zeta}_n = \tilde{h}_n - \tilde{N}_n$
- 357 9. MDT land values are set to NaN.
- 358 10. A spatial filter is applied, if necessary.

359 3.2 Impact of MSS correction onto MDT errors

360 The suggested methodology creating a global MSS is now tested in a practical ex-
 361 ample. We want to obtain an MDT from DTU15 and the TIM_R6 geoid model. Four
 362 approaches to obtain a global MSS are tested:

- 363 1. DTU15 is already a global model and is taken as is.
- 364 2. TIM_R6 is filled in over land. This is the same model that is subtracted from the
 365 MSS to obtain the MDT.
- 366 3. Coastal MDT (ζ_c) is computed by subtracting the GECO geoid model truncated
 367 at maximum d/o 1080 from the MSS. MSS land values are computed following
 368 Eq. 8 applying TIM_R6 for geoid land values $N(x_l)$. This approach minimizes the
 369 error e_c along the coastlines but the missing geoid signal between d/o 301 and 1080
 370 is seen in the MSS land error component e_{N_l} (see Eqs. 10–12).
- 371 4. Coastal MDT ζ_c is computed as in 3, but the GECO geoid model is applied for
 372 land values $N(x_l)$ in Eq. 8. This approach minimizes both e_c and e_{N_l} and is ex-
 373 pectedly the best of the four approaches.

374 The result of the four approaches is displayed in Fig. 1 for the Kuroshio. The first
 375 two approaches (upper two rows in Fig. 1), which both include a step in global MDT
 376 along the coast line, produce false strong MDT gradients near the coast in some regions
 377 and thus unrealistic high surface geostrophic currents. Interestingly, in these approaches
 378 the small-scale wavy structure far away from the coast is also more pronounced than in
 379 the other two methods. This shows that the way the MSS is globalized is not only im-
 380 portant for coastal processes but has also significant offshore effects. If Laplacian smooth-
 381 ing is applied to add a flat MDT signal to the land MSS it remains the choice for the
 382 geoid model added to the MDT signal to obtain the MSS over land. If, in our test case,

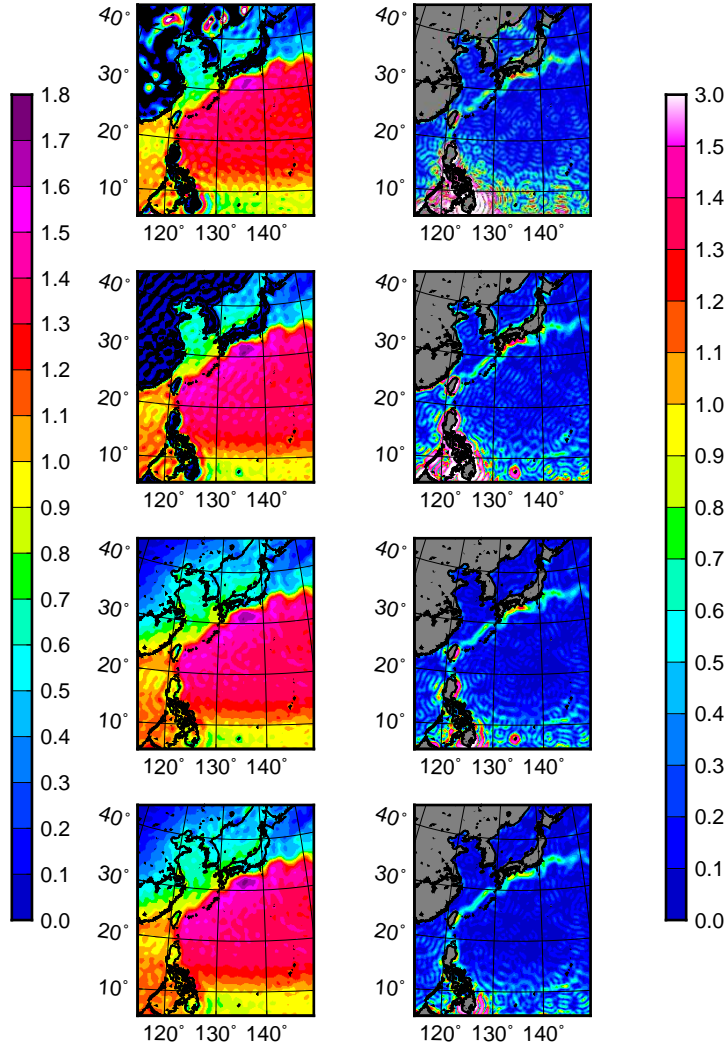


Figure 1. MDT (left, in m) and geostrophic currents (right, in ms^{-1}) as obtained from the four different approaches for land-filling the MSS. Each row refers to one approach in the same order as in the enumerated list in the text.

383 the low resolution TIM_R6 model is applied (third row in Fig. 1) , still unrealistic high
 384 currents result at some individual locations near the coastline, that are not seen when
 385 the high resolution GECO model is applied (bottom row in Fig. 1). In summary, spec-
 386 tral inconsistency of the MSS and the geoid model applied for the land fill-in matters
 387 regionally. But the land-sea step in MDT is clearly the more important issue when glob-
 388 alizing the MSS with impact on the global ocean. We will thus concentrate in the fol-
 389 lowing onto methodologies 1 and 2, which both include the land-sea step, and approach
 390 4, which we propose here as the best strategy for globalizing the MSS.

391 For a specific, regional or global application, the choice of the MDT will depend
 392 on specific criteria or metrics. As a useful example we apply here the comparison to near-
 393 surface drifter data to find the best MDT for two regions (around the Gulf Stream and
 394 the Kuroshio, respectively) and the latitudinal band between 60°S and 60°N. Applying
 395 DTU15 as MSS and TIM_R6 as geoid model as before, two parameters of the MDT com-
 396 putation recipe as listed in section 3 are varied to find that MDT which fits best the drifter
 397 data in the region considered:

- 398 1. the maximum d/o of the MDT
- 399 2. the length scale of the truncated Gaussian kernel applied as spatial filter

400 For all regions the cut-off both at maximum d/o 250 and 300 produces rather large RMS
 401 values below filter length of 0.6° for all three approaches (Fig. 2) and should not be used.
 402 For lower maximum d/o the MDT obtained with approach 4 fits better to the drifter data
 403 for all filter lengths and all regions. Specifically for short filter scales and high d/o needed
 404 to resolve small scale currents, the RMS for approach 4 is much lower than for the other
 405 two approaches. Quality differences of MDTs from approaches 1 and 2 are not that clear.
 406 While globally (60°S-60°N) approach 2 is closer to the drifter data, for the Gulf Stream
 407 and the Kuroshio region RMS values for both methods are rather close.

408 For the Gulf Stream the MDT model following approach 4 with max. d/o 200 and
 409 a filter scale of 0.4° fits best to the drifter data. The best model applying a different MSS
 410 globalization approach is an MDT with max. d/o 250, 0.6° filter scale and following ap-
 411 proach 2. Geostrophic surface currents based on these two MDT models are displayed
 412 in the top panels of Fig. 3. It is clearly seen that, though MSS and geoid include small
 413 scale information up to d/o 250, due to the stronger spatial filtering necessary when ap-
 414 proach 2 is applied, maximum speed in the core of the Gulf Stream is much weaker than
 415 for approach 4. Similar results are found for the Kuroshio (bottom panels of Fig. 4), though
 416 with somewhat smaller differences in velocities from different approaches. The cut-off
 417 maximum d/o is the same as for the Gulf Stream for each of the approaches, respectively
 418 while the filter scales are 0.1° longer.

419 **4 Choice of maximum d/o**

420 For the satellite-only geoid model TIM_R6 we applied in the last section we have
 421 already seen that it isn't recommended to use this model up to its full resolution of d/o
 422 300. Application of other satellite-only geoid models have revealed similar results (Siegismund,
 423 2013). This might be unevitable due to large commission errors in high d/o SH coeffi-
 424 cients, though anisotropic filtering might relax this issue (Bingham, 2010; Cunderlik et
 425 al., 2013). With the usual way of globalizing the MSS, Gibbs effects due to small scale
 426 land signals and the land-ocean step are unevitable. These effects grow with reducing
 427 the spatial resolution of the MDT. Thus, to minimize these effects, a high maximum d/o
 428 is needed, no matter if oceanographic signal is included in the small scales. As an ex-
 429 ample the XGM geoid model is applied to compute (unfiltered) MDTs for maximum d/o
 430 300 to 720 for approaches 1 and 4. Fig. 4 displays the RMS differences of geostrophic
 431 surface currents from these MDTs and the corrected near-surface drifter velocities.

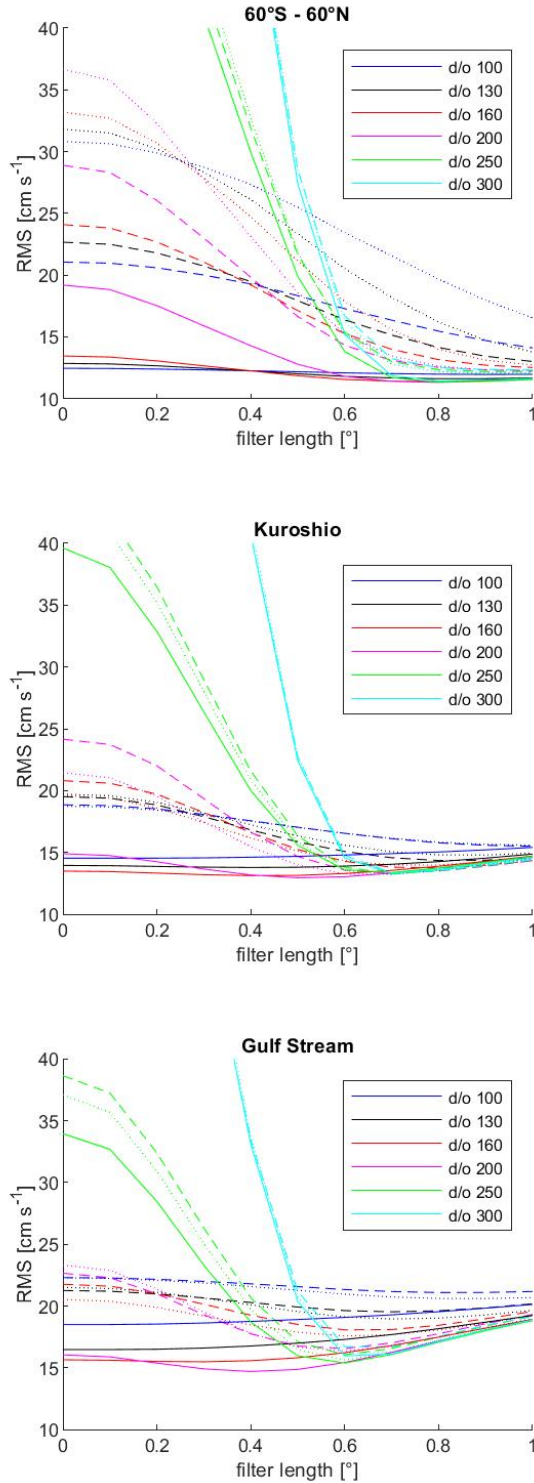


Figure 2. RMS differences [$cm\ s^{-1}$] of geostrophic surface currents as obtained from geodetic MDTs and corrected near-surface drifter velocities. The MDTs are based on TIM_R6 as geoid models and are computed applying approaches $1, 2$ and 4 displayed as dotted, dashed and solid lines, respectively. The three panels show results for (top) the latitudinal band from $60^{\circ}S-60^{\circ}N$, (middle) the Gulf Stream region ($20^{\circ}-40^{\circ}N$, $85^{\circ}-60^{\circ}W$) and (bottom) the Kuroshio ($20^{\circ}-40^{\circ}N$, $120^{\circ}-155^{\circ}E$). For each model and region, MDTs with maximum d/o as listed in the inset and applying a truncated Gaussian filter with filter lengths $[0.0^{\circ}0.1^{\circ}\dots 1.0^{\circ}]$ are tested.

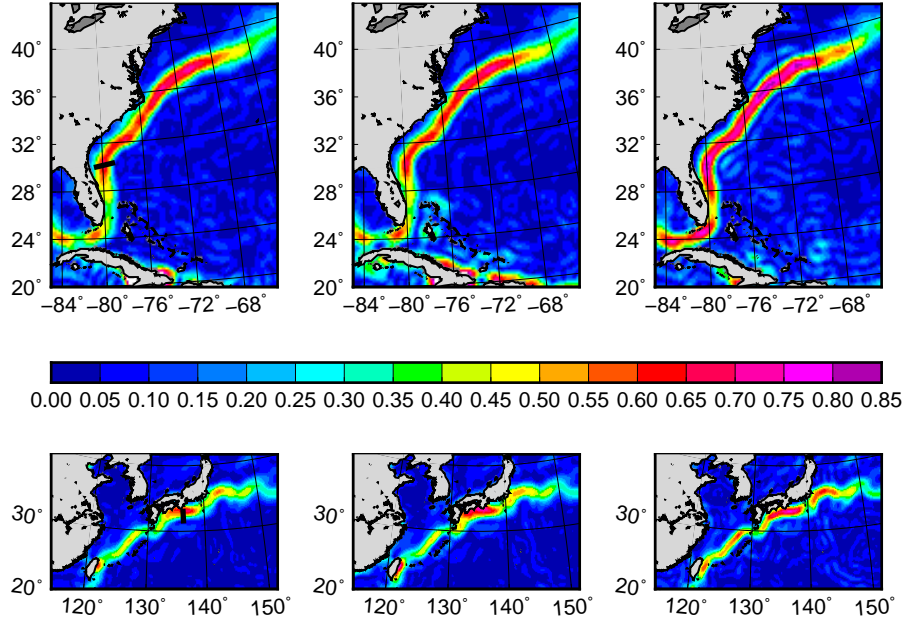


Figure 3. Geostrophic surface velocities [ms^{-1}] from optimized MDT models applying TIM_R6 as geoid model. Optimization is performed for the Gulf Stream region (20° – 40° N, 85° – 60° W, top panels) and the Kuroshio (20° – 40° N, 120° – 155° E, bottom panels) by minimizing the RMS difference to corrected near-surface drifter data with respect to different maximum d/o and spatial filter length applied to the MDT. The optimization is done for each of the MSS globalization approaches. For approach 1 (left) and 2 (center) optimal maximum d/o is 250 for both regions, while filter length is 0.6° (0.7°) for the Gulf Stream (Kuroshio). For approach 4 (right) optimal maximum d/o is 200 for both regions and filter length is 0.4° (0.5°) for the Gulf Stream (Kuroshio). Sections crossing the Gulf Stream (top left) and the Kuroshio (bottom left) are plotted as thick black lines. On these sections direct comparisons of drifter and MDT derived geostrophic (near-)surface currents are performed (see Figs. 5 and 6).

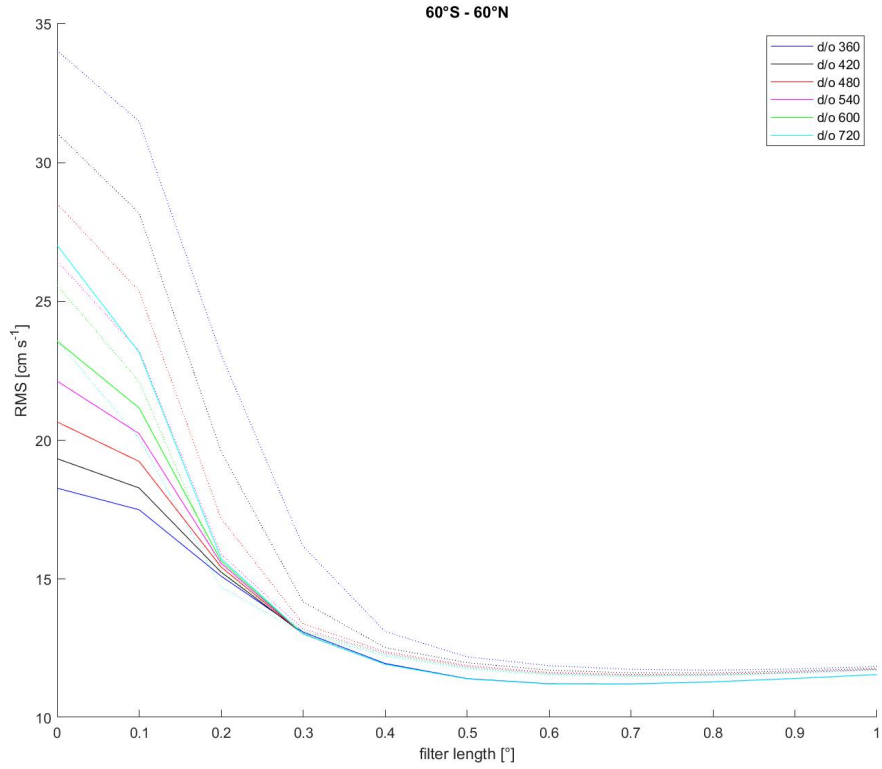


Figure 4. RMS differences [$cm\ s^{-1}$] of geostrophic surface currents as obtained from geodetic MDTs and corrected near-surface drifter velocities for the latitudinal band between 60S–60N. The MDTs include XGM as geoid model and are computed from approaches 1 and 4 displayed as dotted and solid lines, respectively. For both approaches MDTs with maximum d/o as listed in the caption and applying a truncated Gaussian filter with filter lengths [0.0 0.1 ... 1.] are tested.

432 It has to be stated that when considering global performance already for maximum
 433 d/o 300 the bulk of the MDT signal is resolved since most of the global ocean is covered
 434 by large scale gyres rather than small scale currents. Thus, omitted MDT signal is not
 435 a dominant source of error. For approach 4 RMS differences are increasing with max-
 436 imum d/o because of increasing noise in SH coefficients while for approach 1, due to Gibbs
 437 effects, the RMS values are much higher and increase with decreasing maximum d/o.

438 With the Gibbs effects strongly reduced in approach 4 we mainly see the remain-
 439 ing noise in both the geoid model and the MSS and increasing with d/o. Though this
 440 noise is an intrinsic part of available MSS and geoid models, sophisticated anisotropic
 441 filtering might reduce the issue. But it is asked now up to which maximum d/o signal
 442 can be detected in the resulting MDT. With generally growing commission error with
 443 higher d/o it might be advisable to cut the MDT beyond this scale to minimize noise
 444 without loosing signal.

445 To address this question, focus is set on the two strongest western boundary cur-
 446 rents, the Gulf Stream and the Kuroshio. The short across-current scale needs small-scale
 447 information in the MDT to fully resolve the strong gradient in MDT, and the strength
 448 of the currents reduces the influence of the commission error as much as possible. For both
 449 the Gulf Stream and the Kuroshio one section is selected (see Fig. 3, left panels). The
 450 selection is based on the high maximum velocity of the current at this position and the
 451 number of available drifter data, respectively.

452 We compute MDT models applying all six combined geoid models listed in Table
 453 1. For the MDTs that result from subtracting EGM2008, Eigen-6C4, GECO or SGG-
 454 UGM-1 from DTU15 the same geoid model is also used to obtain land geoid values for
 455 DTU15, while for GOCO05c and XGM the GECO model is applied. Spectral resolution
 456 from maximum d/o 100 to d/o 1080 is tested.

457 For the Gulf Stream the MDT obtained from the hydrodynamic GECCO model
 458 is applied for comparison. For this issue the model results are interpolated to a $10' \times 10'$
 459 grid, the same that is used for the geodetic MDTs, and the Laplacian smoother is used
 460 to fill the grid points outside of the North Atlantic. Then the globalized North Atlantic
 461 model is analysed/synthesized to obtain MDTs on the desired maximum d/o.

462 Currents over a section could be characterized either by absolute speed or the ve-
 463 locity component perpendicular to the section. Errors in the MDT will systematically
 464 increase absolute speed assuming independence of the gradients observed in the MDT
 465 and in the error, respectively. To prevent potential bias in geostrophic velocities obtained
 466 from the geodetic MDTs we consider therefore only the speed perpendicular to the sec-
 467 tion with random fluctuations caused by errors in the MDT. The accurate orientation
 468 of the sections is determined by minimizing along-section speed according to the drifter
 469 data.

470 For all MDT models and both sections up to d/o 420 maximum speed increases
 471 with increasing resolution (Figs. 5 and 6). For this resolution maximum velocities have
 472 considerable spread between the different MDT models. For the Gulf Stream (Fig. 5)
 473 they reach between approximately 75 and 90% of maximum velocity observed in the drifter
 474 data. For the Kuroshio (Fig. 6) the geodetic MDTs are very close to the drifter data with
 475 the smallest maximum velocities for GOCO05c and Eigen-6c4 reaching around 93% of
 476 maximum drifter velocity. Beyond d/o 420 the development is heterogeneous but no model
 477 shows substantial increase in maximum velocity. The spatial pattern of the current gen-
 478 erally follows quite closely that observed by the drifter data for the Gulf Stream. Only
 479 the MDT based on the Eigen-6C4 geoid shows higher currents than all other models 50-
 480 100 km offshore the maximum velocity axis. For the Kuroshio the geostrophic currents
 481 from the geodetic MDTs do not follow the velocities observed by the drifters so closely.
 482 Also, beyond d/o 420 a peak of strong velocity develops close to the point of maximum

483 velocity as seen by the drifter data and the structure of the current for resolutions be-
 484 yond max. d/o 720, specifically for max. d/o 1080 is well off the pattern observed by the
 485 drifters. For the Gulf Stream the GECCO maximum velocity increases strongly until d/o
 486 480 and reaches max. around d/o 720 close to max. velocity of the drifter data though
 487 slightly shifted off-coast.

488 To get a clearer view on the development of the MDT-derived geostrophic surface
 489 currents beyond d/o 420 we map the absolute velocities from all four high resolution geoid
 490 models for both the Gulf Stream (Fig. 7) and the Kuroshio (Fig. 8) for max. d/o 420,
 491 max. d/o 1080 and the difference (d/o 1080 - d/o 420). From the comparison of the cur-
 492 rents itself, for both the Gulf Stream and the Kuroshio, the differences in velocities are
 493 hardly detectable. From the mapping of the difference we see for the North Atlantic a
 494 structure that seems to follow the Gulf Stream. However, analysing the geoid height we
 495 see strong gradients east of the North American east coast and differences in the cur-
 496 rents comparing different models beyond d/o 420 seem largely influenced by this effect
 497 in the geoid. Much stronger geoid gradients are found in the Northwest Pacific along the
 498 margin of the Phillipine Plate. Partly this margin follows closely the path of the Kuroshio
 499 and it is not clear whether the differences seen in the currents for different spectral res-
 500 olution is signal in MDT or resolution-dependent spatial patterns caused by the incon-
 501 sistency between geoid and MSS in presence of a strong geoid gradient.

502 5 Conclusions

503 The computation of geodetic MDTs as difference of MSS and geoid needs spectral
 504 consistency of the two fields. Since the geoid is usually derived from Stokes coefficients
 505 describing the geopotential field their natural representation is a linear combination of
 506 SH functions with cut-off at a specific maximum d/o. To obtain the same representa-
 507 tion for the MSS a globalization is needed. This is usually done by filling-in a geoid model
 508 over land. This approach, however, causes unphysical wavy structures in the MDT caused
 509 by the Gibbs phenomenon from the ocean-land discontinuity in the MSS that reflects
 510 the amplitude in coastal MDT, and from spectral inconsistency of the geoid filled in on
 511 land and MSS-MDT over the ocean. The new methodology presented in this paper in-
 512 troduces the MDT as a global field with a continuous ocean-land transition and a flat
 513 definition over land. To obtain an unambiguous global definition the land values of the
 514 DT are defined as the solution of the source-free heat equation with the coastal MDT
 515 as boundary condition. With this definition any ocean MDT can be globalized and res-
 516 olution can be reduced via subsequent SH analysis and synthesis. The land values of the
 517 MSS are consequently defined as sum of global MDT and geoid model. The coastal MDT
 518 values needed to solve the heat equation are obtained from MSS-geoid applying a high
 519 resolution geoid model. The same geoid model is then added to the land MDT to ob-
 520 tain the final MSS values.

521 It is shown that the new methodology reduces strongly the MDT errors near the
 522 coast as well as the unphysical waves offshore. Specifically the ocean-land discontinu-
 523 ity from disregarding the coastal MDT with the sofar used MSS globalization causes in-
 524 creasing MDT errors when spectrally reducing resolution. This feature is vanished with
 525 the new methodology as is shown by comparison with geostrophically corrected near-
 526 surface drifter velocities. Specifically for low maximum d/o the geostrophic velocities from
 527 the MDTs fit now much better to the drifter data if the new method is applied. With
 528 the old method an as high as possible resolution (with the applied geoid model) was gen-
 529 erally necessary to minimize unphysical signals that are caused by both the ocean-land
 530 step and ocean/land geoid spectral inconsistency and which grow with decreasing res-
 531 olution. With this issue strongly diminished, the reduction in spatial resolution is a vi-
 532 able option to reduce the commission error in both geoid and MSS model increasing with
 533 spatial frequency.

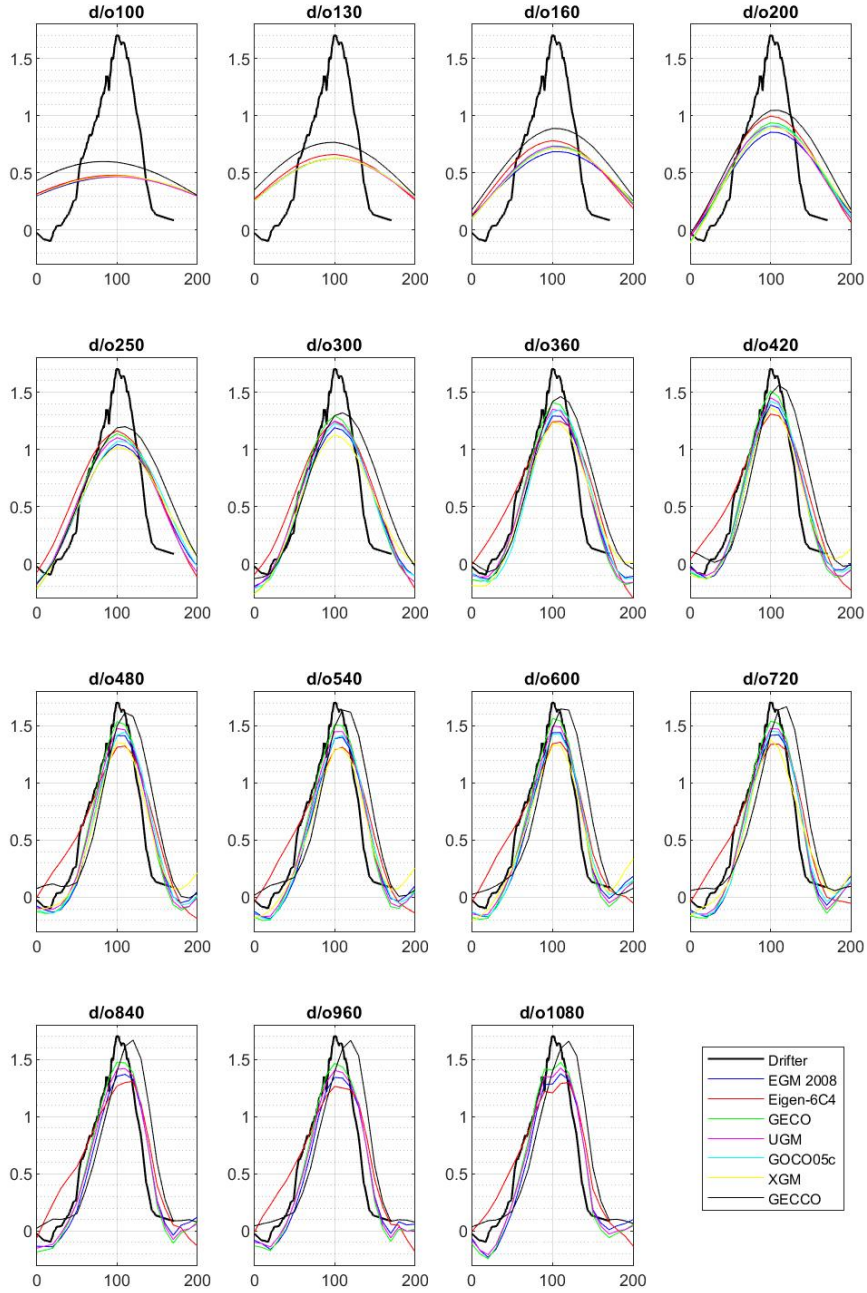


Figure 5. Geostrophic surface velocity [ms^{-1}] over a section across the Gulf Stream (see Fig. 3, top left panel) with the distance over the section provided in [km]. Only the component perpendicular to the section is considered. As listed in the inset, geostrophic surface currents from drifter data and from geodetic and GECCO MDTs are shown. The MDTs are SH analysed/synthesized for a set of selected resolutions from maximum d/o 100 to 1080 each resolution shown in a separate panel.

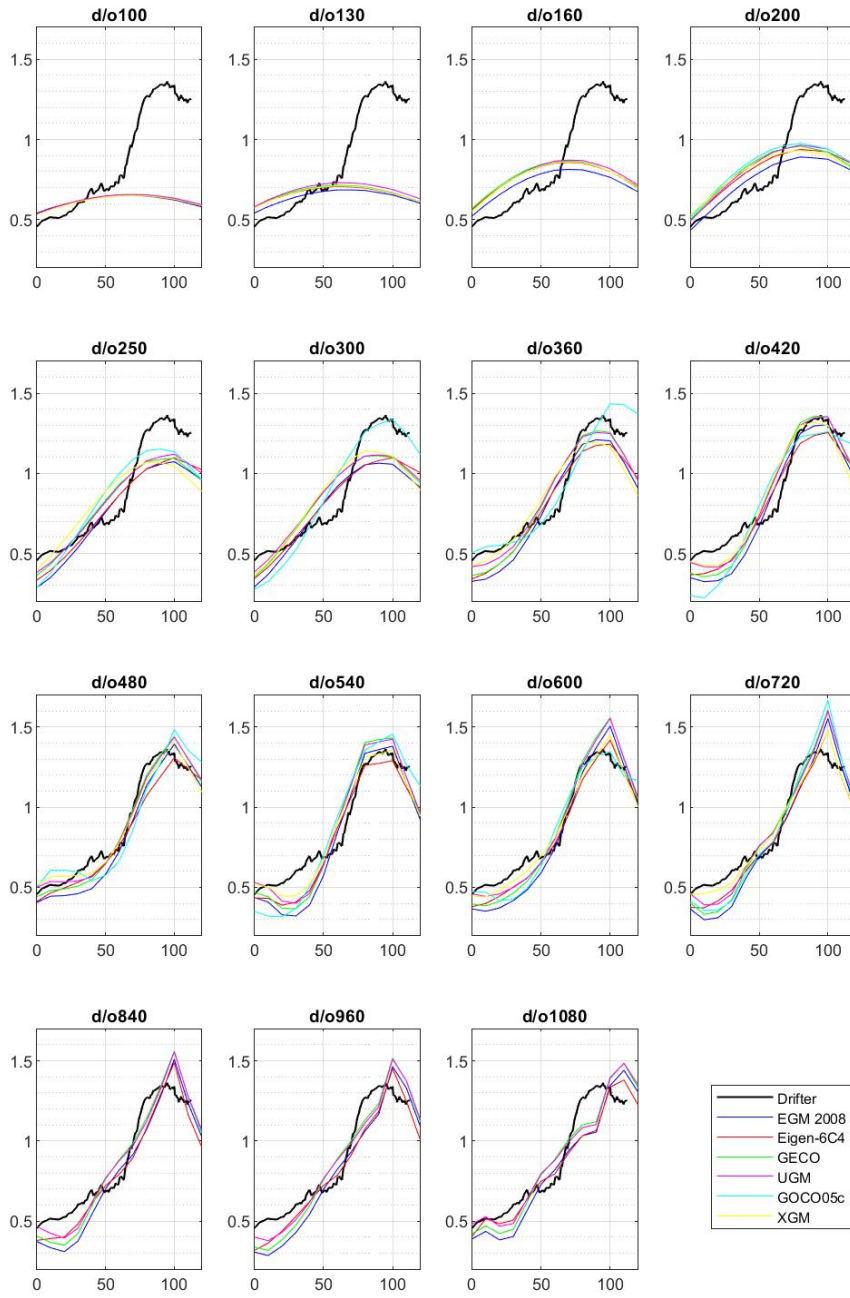


Figure 6. Same as Fig. 5, but for a section over the Kuroshio (see Fig. 3, bottom left panel).

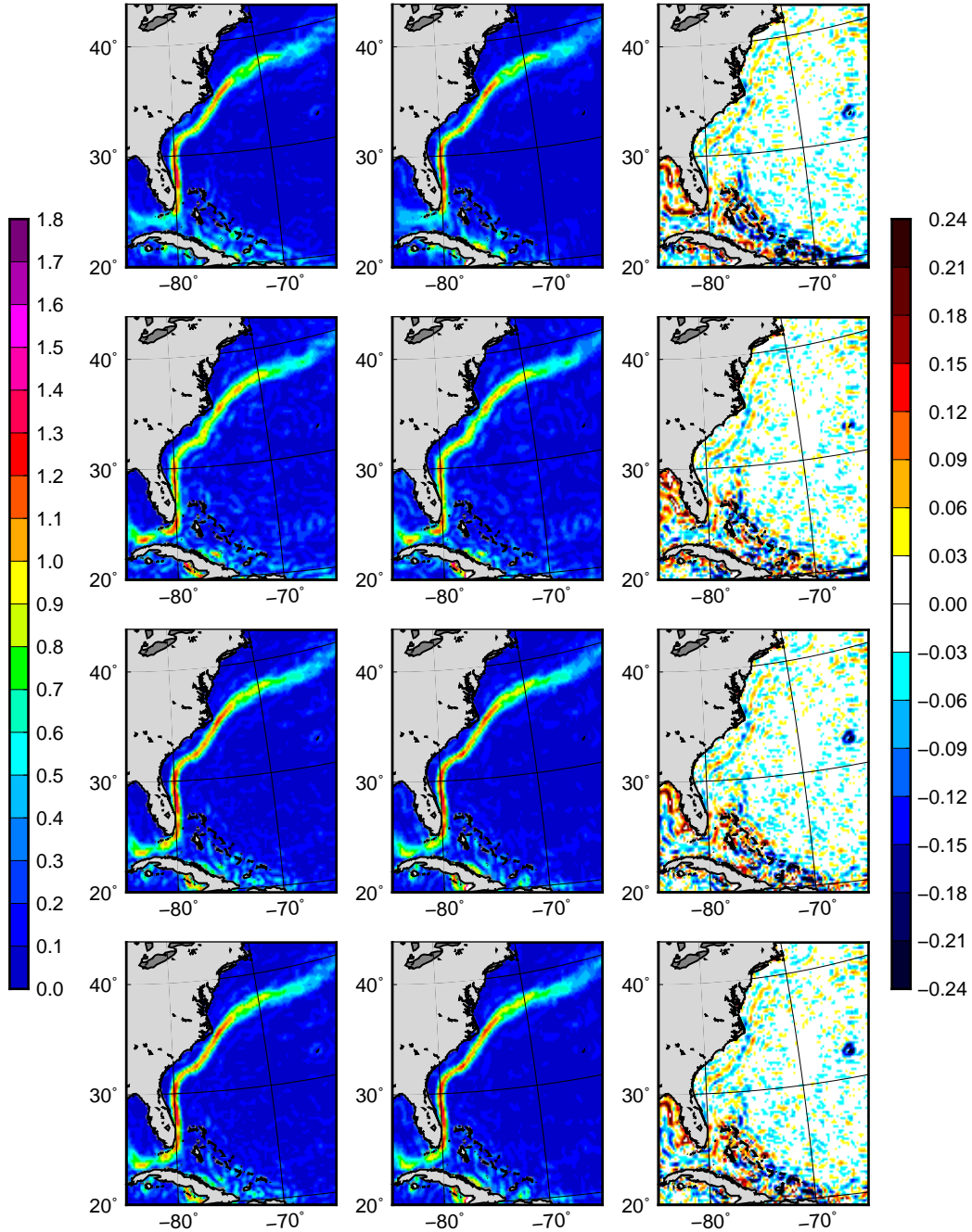


Figure 7. Absolute geostrophic surface currents [ms^{-1}] for the Gulf Stream region from geoidic MDTs applying (from top to bottom) EGM2008, Eigen6C4, GECO and SGG-UGM-1 as geoid models for (left) maximum d/o 420, (middle) d/o 1080 and (right) the difference (d/o 1080-d/o 420). All MDT models are spatially filtered applying a truncated Gaussian kernel with 0.2 filter length.

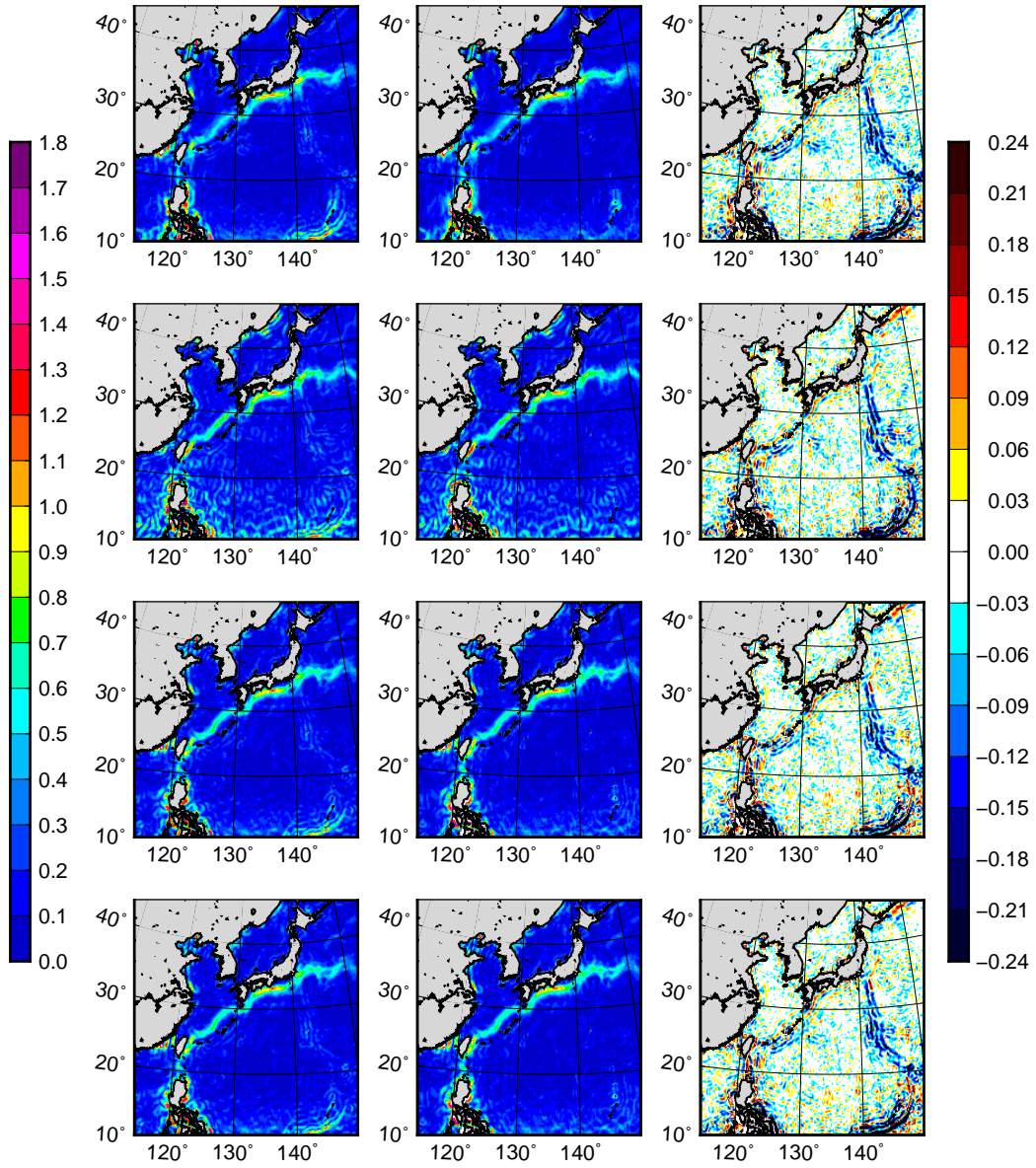


Figure 8. Same as Fig. 7, but for the Kuroshio.

534 To provide assistance for the choice of the MDT spatial resolution in practical ap-
 535 plications, and as an interesting issue by itself, it is tested up to which maximum d/o
 536 physical signal is detectable in MDTs applying recent geoid models and DTU15 as MSS
 537 model. For two sections, one over the Gulf Stream and another one over the Kuroshio
 538 the reconstruction of surface geostrophic velocities is investigated by comparison to drifter
 539 data and results of a high resolution dynamic ocean model. Different resolutions up to
 540 maximum d/o 1080 are tested. Specifically, increasing maximum velocity over the sec-
 541 tion is supposed as indicator that small scale information is added when resolution is in-
 542 creased. It is shown that all MDT models show increasing signal up to d/o 420 for both
 543 sections. Above this resolution, however, the evolution with increasing resolution is not
 544 clear. Strong geoid gradients exist close to both currents. Inconsistencies of MSS and
 545 geoid model seem to cause wavy structures that interfere with the currents generating
 546 spatial patterns depending on resolution. Further investigation is needed.

547 Acknowledgments

548 The sea level anomaly data used in this paper is provided by the Copernicus Marine En-
 549 vironment Monitoring Service (CMEMS). Computations needed to obtain geodetic MDTs
 550 were performed applying the GOCE User Toolbox (GUT) provided by the European Space
 551 Agency (ESA) and available at [https://earth.esa.int/web/guest/software-tools/gut/about-](https://earth.esa.int/web/guest/software-tools/gut/about-gut/overview)
 552 [gut/overview](https://earth.esa.int/web/guest/software-tools/gut/about-gut/overview). Support of the research was provided by the ESA funded project GOCE-
 553 OGMOC (Contract Change Notice No. 9 to Contract No. 18308/04/NL/MM).

554 References

- 555 Albertella, A., & Rummel, R. (2009). On the spectral consistency of the altimet-
 556 ric ocean and geoid surface: a one-dimensional example. *Journal of Geodesy*,
 557 *83*(9), 805–815. (doi: 10.1007/s00190-008-0299-5)
- 558 Andersen, O. B., Stenseng, L., Piccioni, G., & Knudsen, P. (2016). The dtu15 mss
 559 (mean sea surface) and dtu15lat (lowest astronomical tide) reference surface.
 560 In *Esa living planet symposium 2016, prague, czech republic*.
- 561 Bingham, R. (2010).
 562 *Remote Sensing Letters*, *1:4*, 205–212. (doi:10.1080/01431161003743165)
- 563 Bingham, R., Haines, K., & Hughes, C. W. (2008). Calculating the ocean’s mean
 564 dynamic topography from a mean sea surface and a geoid. *Journal of Atmo-*
 565 *spheric and Oceanic Technology*, *25*(10), 1808–1822. (doi: 10.1175/2008JTE-
 566 *CHO568.1*)
- 567 Biri, S., Serra, N., Scharffenberg, M. G., & Stammer, D. (2016). Atlantic sea surface
 568 height and velocity spectra inferred from satellite altimetry and a hierarchy
 569 of numerical simulations. *J. Geophys. Res. Oceans*, *121*, 4157–4177. doi:
 570 10.1002/2015JC011503
- 571 Boyer, T. P., Levitus, S., Garcia, H., Locarnini, R., Stephens, C., & Antonov, J.
 572 (2005). Objective analyses of annual, seasonal, and monthly temperature and
 573 salinity for the world ocean on a 0.25 grid. *Int. J. Climatol.*, *25*(7), 931–945.
- 574 Brockmann, J. M., Zehentner, N., Hock, E., Pail, R., Loth, I., Mayer-Gurr, T., &
 575 Schuh, W. D. (2014). Egm.tim.rl05: An independent geoid with centimeter
 576 accuracy purely based on the goce mission. *Geophysical Research Letters*,
 577 *41*(22), 8089–8099. doi: 10.1002/2014gl061904
- 578 Cunderlik, R., Mikula, K., & Tunega, M. (2013). Nonlinear diffusion filtering of data
 579 on the earth’s surface. *J. Geod.*, *87*, 143–160. (doi: 10.1007/s00190-012-0587-
 580 *y*)
- 581 Dee, D. P., et al. (2011). The era-interim reanalysis: configuration and performance
 582 of the data assimilation system. *Quarterly Journal of the Royal Meteorological*
 583 *Society*, *137*(656), 553–597. doi: 10.1002/qj.828

- 584 Fecher, T., Pail, R., Gruber, T., & the GOCO consortium. (2017). Goco05c: A new
 585 combined gravity field model based on full normal equations and regionally
 586 varying weighting. *Surveys in Geophysics*, *38*(3), 571–590.
- 587 Feng, G., Jin, S., & Sanchez-Reales, J. M. (2013). Antarctic circumpolar current
 588 from satellite gravimetric models itg-grace2010, goce-tim3 and satellite altimetry.
 589 *Journal of Geodynamics*, *72*, 72–80.
- 590 Frst, C., Bruinsma, S. L., Abrikosov, O., Lemoine, J.-M., Marty, J. C., Flechtner,
 591 F., ... Biancale, R. (2014). *Eigen-6c4 the latest combined global gravity field
 592 model including goce data up to degree and order 2190 of gfz potsdam and grgs
 593 toulouse* (Tech. Rep.). GFZ German Research Centre for Geosciences. (doi:
 594 10.5880/ICGEM.2015.1)
- 595 Gilardoni, M., Reguzzoni, M., & Sampietro, D. (2016). Geco: a global gravity model
 596 by locally combining goce data and egm2008. *Studia Geophysica et Geodaetica*,
 597 *60*, 228–247. doi: 10.1007/s11200-015-1114-4
- 598 Kalnay, et al. (1996). The ncep/ncar 40-year reanalysis project. *Bull. Amer. Meteor.
 599 Soc.*, *77*, 437–470.
- 600 Knudsen, P., Bingham, R., Andersen, O., & Rio, M. H. (2011). A global mean dy-
 601 namic topography and ocean circulation estimation using a preliminary goce
 602 gravity model. *Journal of Geodesy*, *85*, 861–879. (doi: 10.1007/s00190-011-
 603 0485-8)
- 604 Liang, W., Xu, X., Li, J., & Zhu, G. (2018). The determination of an ultra high
 605 gravity field model sgg-ugm-1 by combining egm2008 gravity anomaly and
 606 goce observation data. *Acta Geodaetica et Cartographica Sinica*, *47*(4), 425–
 607 434. doi: 10.11947/j.AGCS.2018.20170269
- 608 Lumpkin, R., & Johnson, G. C. (2013). Global ocean surface velocities from
 609 drifters: Mean, variance, el niño-southern oscillation response, and seasonal
 610 cycle. *Journal of Geophysical Research: Oceans*, *118*, 2992–3006. doi:
 611 10.1002/jgrc.20210
- 612 Lumpkin, R., & Pazos, M. C. (2007). Measuring surface currents with surface ve-
 613 locity program drifters: The instrument, its data, and some recent results. In
 614 *Lagrangian analysis and prediction of coastal and ocean dynamics* (pp. 39–67).
 615 Cambridge University Press.
- 616 Marshall, J., Hill, C., Perelman, L., & Adcroft, A. (1997). Hydrostatic, quasi-
 617 hydrostatic and nonhydrostatic ocean modelling. *J. Geophys. Res.*, *102*,
 618 5733–5752.
- 619 Maximenko, N. (2004). Correspondence between lagrangian and eulerian velocity
 620 statistics at the asuka line. *J. Oceanography*, *60*, 681–687.
- 621 Pail, R., Fecher, T., Barnes, D., Factor, J. F., Holmes, S. A., Gruber, T., & Zingerle,
 622 P. (2018). Short note: the experimental geopotential model xgm2016. *Journal
 623 of Geodesy*, *92*(4), 443–451.
- 624 Pavlis, N. K., Holmes, S. A., Kenyon, S. C., & Factor, J. K. (2012). The develop-
 625 ment and evaluation of the earth gravitational model 2008 (egm2008). *Journal
 626 of Geophysical Research*, *117*. (B04406) doi: 10.1029/2011JB008916
- 627 Ralph, E. A., & Niiler, P. (1999). Wind-driven currents in the tropical pacific. *Jour-
 628 nal of Physical Oceanography*, *29*, 2121–2129.
- 629 Rio, M.-H., & Hernandez, F. (2003). High-frequency response of wind-driven cur-
 630 rents measured by drifting buoys and altimetry over the world ocean. *Journal
 631 of Geophysical Research*, *108*(C8). doi: 10.1029/2002JC001655
- 632 Rummel, R., Balmino, G., Johannessen, J., Visser, P., & Woodworth, P. (2002).
 633 Dedicated gravity field missions - principles and aims. *Journal of Geodynam-
 634 ics*, *33*(1–2), 3–20.
- 635 Sanchez-Reales, J. M., Andersen, O. B., & Vig, M. I. (2016). Improving surface
 636 geostrophic current from a goce-derived mean dynamic topography using
 637 edge-enhancing diffusion filtering. *Pure Appl. Geophys.*, *173*, 871–884. (doi
 638 10.1007/s00024-015-1050-9)

- 639 Sanchez-Reales, J. M., Vigo, M. I., Jin, S., & Chao, B. (2013). Global surface
640 geostrophic ocean currents derived from satellite altimetry and geoid.
641 *Marine Geodesy*, *35*(S1), 175–189. (doi: 10.1080/01490419.2012.718696)
- 642 Siegmund, F. (2013). Assessment of optimally filtered recent geodetic mean dy-
643 namic topographies. *Journal of Geophysical Research: Oceans*, *118*, 108–117.
644 doi: 10.1029/2012JC008149
- 645 Tapley, B. D., Bettadpur, S., Watkins, M. M., & Reigber, C. (2004). The gravity
646 recovery and climate experiment: mission overview and early results. *Geophys.*
647 *Res. Lett.*, *31*. (L09607 , doi:10.1029/2004GL019920)